Subband-Landau-level spectroscopy in GaAs-$Al_xGa_{1-x}As$ heterojunctions

G. L. J. A. Rikken,* H. Sigg,† C. J. G. M. Langerak, H. W. Myron, and J. A. A. J. Perenboom
High Field Magnet Laboratory and Research Institute for Materials, University of Nijmegen, Toernooiveld, NL-6525 ED Nijmegen, The Netherlands

G. Weimann
Forschungsinstitut der Deutschen Bundespost beim Fernmeldtechnischen Zentralamt, D-6100 Darmstadt, Federal Republic of Germany
(Received 26 June 1986)

Resonant coupling of the subband Landau levels in the two-dimensional electron gas of high-mobility GaAs-$Al_xGa_{1-x}As$ heterojunctions has been measured, and a detailed analysis is presented. We have investigated the subband structure and the coupling strength using cyclotron resonance at energies near the transition energy between the subband levels. This was done at constant magnetic field for a range of energies by far-infrared interferometry, and for a fixed energy of incident radiation while varying the strength of the applied magnetic field. In both cases, a broadening and splitting of the cyclotron resonance line were observed. We show that one thus directly obtains the subband transition energy and the coupling strength which depend strongly on the shape of the interface potential. Calculations of the hybridization of the subband Landau levels, based on a triangular potential well, result in an energy, field, and angle dependence of the coupling in good agreement with experimental observations and reproduce the double resonance observed at a fixed energy of laser radiation. The electron concentration was influenced either by illuminating the sample or by applying a back gate voltage on the GaAs substrate, and the resulting variation of the transition energy is found to be in accordance with the results of self-consistent calculations.

I. INTRODUCTION

For a quantitative understanding of the properties of the two-dimensional electron gas (2D EG), accurate and reliable values for subband transition energies E_{nm} and for the spatial extension of the subband wave functions are of great importance. From a comparison of measured subband transition energies with model calculations of the electronic band structure of the interface[1] the details of the confining interface potential can be sensitively determined. Various experimental techniques have already been developed to study the subband energy-level structure of the 2D EG, such as absorption spectroscopy[2,3] and intersubband-cyclotron combined resonance.[4]

Schlesinger, Hwang, and Allen[5] introduced the novel technique of resonant subband-Landau-level coupling (RSLC): A small component of the applied magnetic field parallel to the interface will lift any degeneracy of the subband Landau levels and lead to hybridization of Landau levels belonging to different subbands. A splitting of the cyclotron resonance (CR) is then observed when the CR energy $\hbar\omega_c$ coincides with a subband transition energy E_{nm}.

We observed a splitting of the CR using incident radiation of fixed energy for a particular value of the electron concentration (cf. Fig. 1); this effect was attributed to a coupling between the $N=1$ Landau level of the lowest subband and the $N=0$ Landau level of the first excited subband.[6] It is most remarkable that two resonances belonging to the lower and upper branch of the hybridized subband Landau levels are simultaneously observed at the same energy; this indicates that for a proper understanding linewidth effects have to be taken into consideration.

In this paper we will present new measurements of RSLC in GaAs-$Al_xGa_{1-x}As$ heterojunctions, and we will show that from the subband transition energy and coupling strength, determined in these measurements, de-

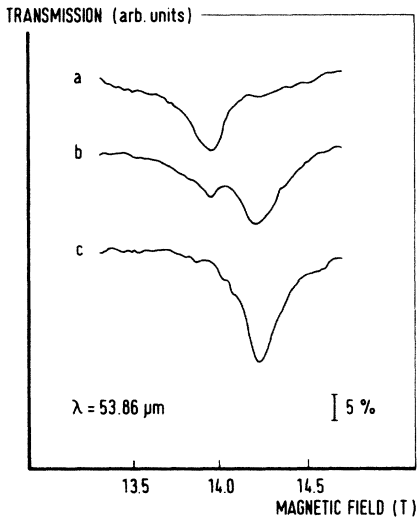

FIG. 1. Transmission at a laser wavelength $\lambda=53.86$ μm with the magnetic field tilted $\theta=2.5°$ from the normal to the 2D EG. The curves correspond to different values of the back gate voltage: (a) $V_g=20$ V; (b) $V_g=0$ V; (c) $V_g=-20$ V.

tailed information on the shape of the interface potential can be deduced. The experimental details are described in Sec. II. Section III gives model calculations of the subband-Landau-level coupling based on a triangular well potential. In Secs. IV A and IV B the measurements are reported to be obtained at a fixed strength of the magnetic field and at a fixed energy of the incident radiation, respectively. The subband transition energy and the coupling strength are determined. The field and angle dependence of the coupling of the subband Landau levels is compared with the predictions of our triangular well model. Also, the changes in transition energy and coupling strength are discussed resulting from the variation of the electron density and of the shape of the potential well by either a back gate voltage or illumination of the device. In Sec. V, finally, we will discuss how the incorporation of broadening of the Landau levels will allow to reproduce the features of the CR splitting of Fig. 1.

II. EXPERIMENTAL

The measurements were performed on high mobility, molecular-beam epitaxy (MBE) grown, modulation doped GaAs-$Al_{0.3}Ga_{0.7}As$ heterojunctions[7] with electron concentration of the order of 2×10^{11} cm^{-2}. The 300 μm-thick substrates were wedged to eliminate interference effects. A 6 μm-thick Mylar foil onto which a 15-nm-thick Cr layer had been evaporated served as a semitransparent back gate to enable us to apply electric fields of a few times 10^6 V/m at the interface. Using this back gate we could vary the 2D electron concentration by approximately 20%; the electron concentration was also varied by means of illumination with a red light-emitting diode (LED). The electron concentration was determined each time from the low-field Shubnikov—de Haas oscillations.

The samples were immersed in a pumped liquid-helium bath at $T\approx1.3$ K and could be rotated over an angle θ up to 15 deg around an axis perpendicular to the magnetic field. The beam of far-infrared (FIR) radiation, incident to the sample, was parallel to the applied magnetic field; its transmission through the samples was detected by a carbon bolometer mounted in an integrating sphere immediately below the sample. The magnetic field was generated with a 15-T Bitter magnet.

Measurements were performed at constant applied magnetic field using a Michelson interferometer. Figure 2 gives a set of spectra of the CR transmission of a sample for which the normal to the interface was tilted over $\theta=3.8°$ from the direction of the magnetic field. For the low and high values of the magnetic field, only one resonance line is well developed. As the field increases the lower-energy resonance becomes less pronounced and a higher-energy resonance starts to develop; when, around 12.2 T, the field reaches a value for which the undisturbed CR energy would have been equal to E_{10} the two resonances are of equal strength, and for high enough field only the uppermost resonance will remain. The doublet splitting turns out to be proportional to the component of the magnetic field parallel to the interface. These spectra are a good tool to determine the value of E_{10} and the magnitude of the splitting of the CR as we will elaborate

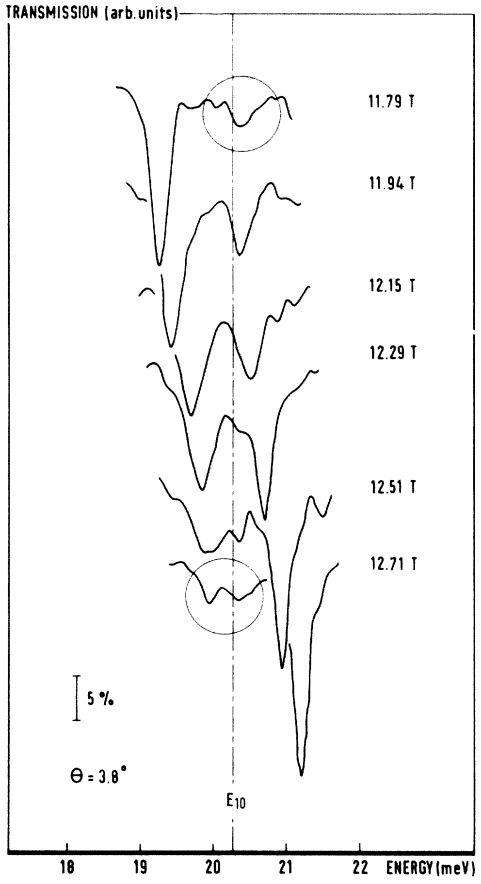

FIG. 2. Transmission spectra measured using a far-infrared interferometer for various values of the magnetic field, with the axis of the applied field tilted $\theta=3.8°$ from the normal to the 2D EG.

in Sec. IV. For an analysis of the CR linewidth, however, the higher energy resolution and the higher intensity of the radiation obtained with a laser are of great advantage.[8]

Far-infrared radiation with a power of typically a few milliwatts is generated by an optically pumped molecular gas laser at discrete wavelengths. The accessible laser lines are so widely spaced that in general no laser line will be found close enough to the subband transition energy to directly observe the small splitting of the CR due to RSLC. By means of an electric field through the application of a back gate voltage, however, the electron concentration and the subband energies can be varied and in this way E_{10} can be made to coincide with the energy of the incident FIR laser radiation. It is observed, as in Fig. 1, that with decreasing back gate voltage (i.e., with increasing subband transition energy) one CR mode will broaden and shift to lower magnetic fields while a higher-field mode will develop and become narrower as it shifts towards the unperturbed resonance field $B=(m^*/\hbar e)\hbar\omega_c$. Still it is remarkable that the two modes belonging to the upper and lower branch of the hybridized subband Landau levels are observed simultaneously. This fact becomes clear when we consider Fig. 2 in more detail. Let us focus our attention on the transmission at the energy of the in-

cident laser radiation, which is supposed to be close to E_{10}. The unperturbed CR would be in resonance with the subband transition energy around 12.2 T. From the spectra of Fig. 2 absorption is found at magnetic fields close to but below this resonance field due to the tail of the high-energy line of the doublet (cf. circle for 11.79 T); for increasing magnetic fields this absorption will pass through a maximum and the tail of the low-energy line will gradually start to contribute to the absorption until for fields above 12.7 T no appreciable absorption will be left (cf. circle for 12.71 T). The details of the resonances as observed in Fig. 1, such as their splitting, depend in a very complicated way on the linewidth of the CR and therefore on the broadening of the subband Landau levels. In the following we will first try to understand the RSLC neglecting these line-broadening effects, these will be discussed later in Sec. V.

III. COUPLING CALCULATIONS

In order to understand the results shown above in a more quantitative fashion we have calculated the subband-Landau-level coupling. For such calculations one of course requires the subband energies and wave functions. For simplicity, we perform our calculations in the one-electron approximation and use a simple triangular potential well with a conveniently chosen slope instead of using a self-consistent potential approach.[1,9] We feel that this simplified picture contains the principal physical features of the problem which is confirmed by the agreement with the experimental data.

The problem reduces to finding the eigenvalues of the well-known Hamiltonian

$$H=\frac{1}{2m}[(p_x+eBz\sin\theta)^2+(p_y+eBz\cos\theta)^2+p_z^2]+e\lambda z \ , \tag{1}$$

where the z axis is perpendicular to the interface of the heterojunction, the magnetic field is tilted from the z axis over an angle θ, and λ determines the slope of the triangular potential. The Hamiltonian can be separated into $H=H_{||}+H_{\perp}+H'$.[10]

We will choose as a basis

$$\psi_{nNX}(\mathbf{r},z)=\frac{1}{\sqrt{L}}\exp\left[-i\frac{Xy}{l_{\perp}^2}-i\frac{z_{nn}(x-X)}{l_{||}^2}\right]$$
$$\times\chi_N(x-X)\zeta_n(z) \ , \tag{2}$$

where $l_{\perp}^2=\hbar/eB\cos\theta$, $l_{||}^2=\hbar/eB\sin\theta$; the matrix elements z_{nm} are defined by

$$z_{nm}=\int_0^{\infty}\zeta_n^*(z)z\zeta_m(z)dz \ . \tag{3}$$

The in-plane wave functions $\chi_N(x-X)$ are the eigenfunctions of $H_{||}$ and are the usual Landau-level wave functions:

$$\chi_N(x)=i^N[2^N(N!)\sqrt{\pi}l_{\perp}]^{-1/2}H_N(x/l_{\perp})$$
$$\times\exp(-x^2/2l_{\perp}^2) \ , \tag{4}$$

where $H_N(x)$ is the Hermite polynomial. The wave functions perpendicular to the interface, $\zeta_n(z)$, are chosen real and satisfy:

$$H_{\perp}\zeta_n(z)=\left[\frac{p_z^2}{2m}+e\lambda z+\frac{\hbar^2z^2}{2ml_{||}^4}\right]\zeta_n(z)$$
$$=E_n(B\sin\theta)\zeta_n(z) \ . \tag{5}$$

The term in the Hamiltonian that will lead to a coupling of the motion in the plane of the 2D EG with the motion along the z axis is

$$H'=\frac{\hbar}{m}\frac{zp_x}{l_{||}^2} \ . \tag{6}$$

This term is zero when the applied magnetic field has no component parallel to the 2D EG. The matrix elements $\langle n',N',X'\,|\,H\,|\,n,N,X\rangle$ are worked out in Ref. 10, and can be evaluated easily in the case of a triangular potential well. This matrix was numerically diagonalized, and the five lowest subbands ($n=0,1,\ldots,4$) and from every subband the five lowest Landau levels $|\,n,N\rangle$ ($N=0,1,\ldots,4$), were taken into account in order to ensure convergence. The eigenfunctions of the Hamiltonian, including the coupling through H', will be linear combinations of the wave functions of Eq. (2), and we will denote these by ψ_i.

Figure 3 shows a result where the electric field λ is

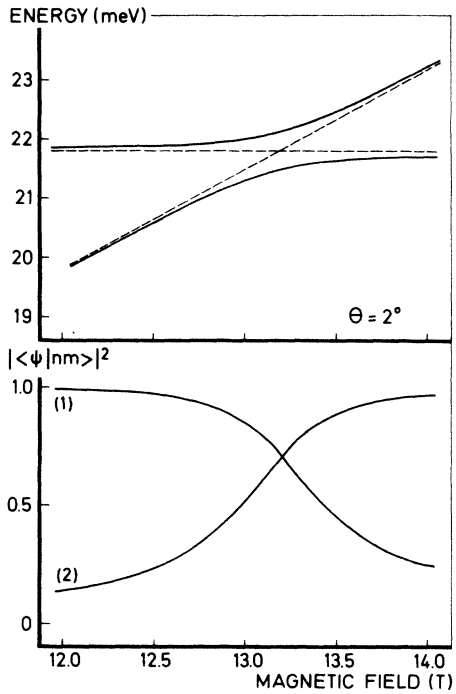

FIG. 3. The transition energy relative to the energy of the lowest Landau level calculated for a triangular well potential for $\theta=2°$, and projections $|\langle\psi\,|\,n,m\rangle|^2$ of the eigenstates on the pure subband-Landau-level states $|\,n,N\rangle$; (1), $|\langle\psi_1\,|\,0,1\rangle|^2$ and (2), $|\langle\psi_1\,|\,1,0\rangle|^2$. Within the resolution of this graph $|\langle\psi_2\,|\,1,0\rangle|^2=|\langle\psi_1\,|\,0,1\rangle|^2$ and $|\langle\psi_2\,|\,0,1\rangle|^2=|\langle\psi_1\,|\,1,0\rangle|^2$.

chosen to give a crossing of $|0,1\rangle$ and $|1,0\rangle$ at 13.2 T. The splitting observed for a particular strength of the magnetic field is due to the two branches of the subband-Landau-level coupled CR energy and the two transmission peaks will have a strength proportional to the two projections $|\langle\psi|0,1\rangle|^2$ and $|\langle\psi|1,0\rangle|^2$ given in Fig. 3. It should be noted that there is already a significant mixing of states when the eigenvalue is still close to its unperturbed value. It is because of this that for fixed energy of the incident radiation we can observe two minima in the transmission, one at a magnetic field below and one above the crossing field.

IV. DISCUSSION

A. Interferometer measurements

Figure 2 shows that near the subband transition energy two CR lines can be found; their energies are plotted as a function of magnetic field in Fig. 4. The midpoints of the pairs of resonances are given as well, and from the intersection with the line $\hbar\omega_c=(e\hbar/m^*)B$ the resonance field of the subband transition energy will be found. In fact, we determined the effective mass m^* from resonances far away from the anti-level-crossing [Fig. 4(b)]. At the resonance field, the two transmission minima are of equal strength and the observed splitting is reaching a minimum. This procedure is consistent with the theoretical analysis of the foregoing section and allows a very accurate determination of the resonance field.

Figure 5 shows the angle dependence of the splitting at the resonance field; the point-dashed line corresponds to our calculations based on a triangular well potential; the solid line corresponds to the harmonic oscillator model of Ref. 5. The triangular potential-well approximation is in much better agreement with the experiment than the harmonic-oscillator model.

We have determined the subband splitting for several samples under different conditions. These conditions are listed in the inset of Fig. 6. The coupling strength is taken as the derivative of the subband splitting with respect to the tilt angle and normalized to the subband transition energy: $(\partial\Delta E/\partial\theta)/E_{10}$. Figure 6 gives the coupling strength plotted as a function of E_{10}. Both the subband splitting and E_{10} seem to depend on the initial conditions, like the cooling cycle. The triangular potential-well approximation used here, gives a coupling strength 0.871, independent of E_{10}, while in the case of the harmonic-oscillator potential of Ref. 5, the coupling strength would be $\sqrt{2}$. It is found in Fig. 6 that the coupling strength becomes smaller with increasing back gate voltage. This can be understood as follows: Inspection of Eq. (6) shows that in the limit $\sin\theta \ll 1$ $(\partial\Delta E/\partial\theta)/E_{10}$ is proportional to z_{10}, the overlap matrix element defined in Eq. (3). From simple electrostatic considerations it is expected that the interface potential will bend off at its back gate side due to the applied positive back gate voltage. The wave function $\zeta_1(z)$ will then extend further into the GaAs layer than $\zeta_0(z)$ and therefore the matrix element z_{10}, and consequently the coupling strength, will be reduced. But when the sample is illuminated with a red light-emitting diode (LED) (from 1 to 4 in Fig. 6), the subband coupling strength is found to stay approximately constant while the subband transition energy is increased. It implies that in this case the shape of the potential is much less affected.[11]

The maximum value of the coupling strength found in

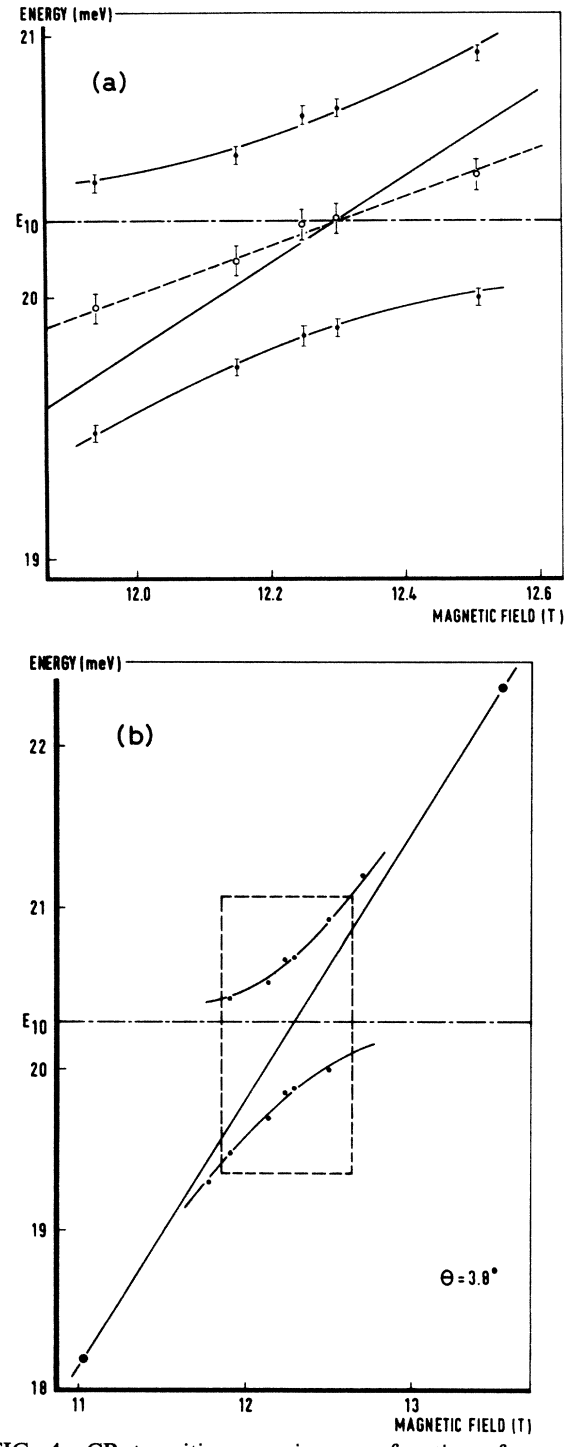

FIG. 4. CR transition energies as a function of magnetic field, as obtained from the spectra of Fig. 2; (a) E_{10} is found from the midpoints of the pairs of resonances (open circles) and the effective mass line. (b) The effective-mass line is determined from measurements far away from the anti-level-crossing.

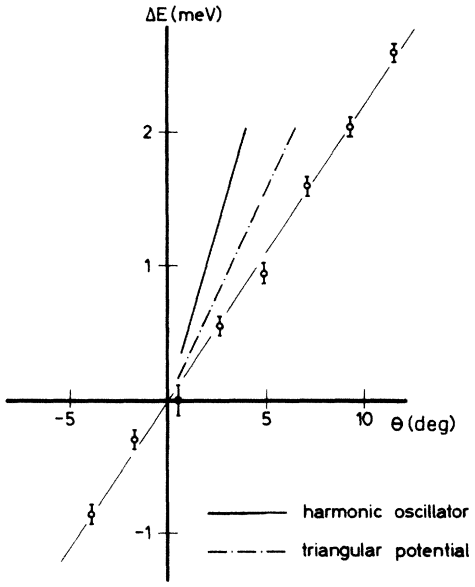

FIG. 5. The angle dependence of the splitting. The measurements are indicated by open circles. The solid and point-dashed lines correspond to the calculations with the harmonic-oscillator and triangular potential-well approximation, respectively.

Fig. 6 is lower than that calculated from the triangular potential-well approximation. This is also true for the data of Schlesinger, Hwang, and Allen,[5] from their Fig. 4 one can find a coupling strength of 0.77. One is tempted to attribute this difference to depolarization and excitonlike effects. Recently, Zaluzny showed that the transition energy measured by RSLC is the depolarization shifted electric subband transition energy $\tilde{E}_{10}=E_{10}(1+\gamma_{11}/2)$ where γ_{11} determines the strength of depolarization and excitonlike effects.[12] A positive value for γ_{11} would increase the coupling strength and improve the agreement with the simple model used, since in our work the coupling strength involves a normalization with $\tilde{E}_{10}$. We feel however, that the triangular potential-well approximation is not accurate enough to allow one to deduce a value for γ_{11} from these data.

In principle, one could find a more realistic potential from a subband calculation, where the interface potential given by the Poisson equation is self-consistently included in the Hamiltonian of Eq. (1). We will not attempt to extend our simple model. Instead, we compare our experimental results with the self-consistent calculations recently published by Stern and Das Sarma.[9]

In Fig. 7, E_{10} is plotted as a function of the 2D electron concentration n for the different conditions summarized in Fig. 6. With increasing back gate voltage V_g, n is found to increase to a saturation value of approximately 2.6×10^{11} cm^{-2}. A higher electron concentration is obtained by photoexcitation of charge carriers when the sample is illuminated with a LED. Figure 7 clearly shows that the subband transition energy decreases when the electron concentration is increased with an applied back gate voltage. In contrast, an increase of the carrier concentration through illumination (point 4) leads to an increase of E_{10}. This shows again that entirely different mechanisms are in play to change the carrier concentration of the 2D EG.

With photoexcitation one produces a transfer of charge from the $Al_xGa_{1-x}As$ layer to the GaAs layer,[13] this will lead to an increase of the space-charge layer and conse-

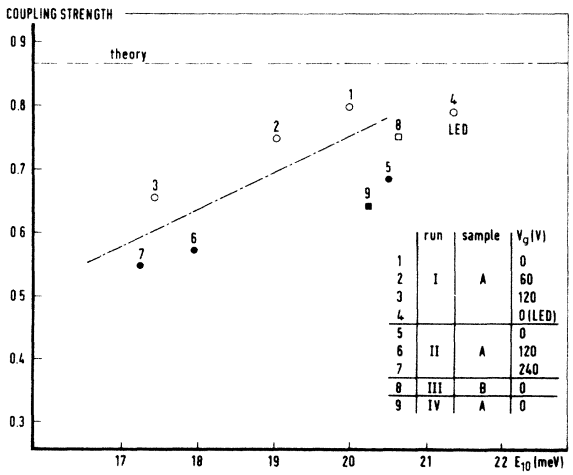

FIG. 6. The coupling strength $(\partial\Delta E/\partial\theta)/E_{10}$ as a function of E_{10}. In the inset the references to sample and back gate voltages are given.

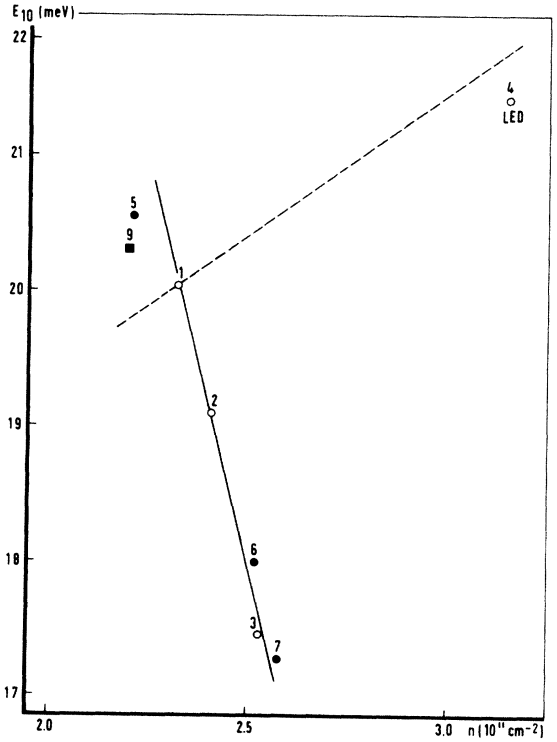

FIG. 7. Subband transition energy E_{10} as a function of the electron density n. The numbers refer to the list in Fig. 6. The solid line and the dashed line are calculated from Ref. 9.

quently to an increase of the electric field at the interface. This will cause E_{10} to increase, as is confirmed by Stern and Das Sarma.[9] Their results for E_{10}, as a function of the electron concentration, are shown by the dashed line in Fig. 7. To reproduce the value of E_{10} for point 1, we had to assume a value for the unintentional background doping of 2×10^{14} cm^{-3}, a reasonable value compared to doping values found for such heterojunctions.[7]

By applying a back gate voltage, an additional electron concentration Δn can be introduced into the channel of the 2D EG, but in this case there is no charge flow from the $Al_xGa_{1-x}As$ through the interface.[14] In this case and from a simple application of Poisson's equation, one finds an induced electric field between the channel and the back gate (BG) of $\Delta F_{BG}=-e\,\Delta n/\epsilon$, where ϵ is the dielectric constant for GaAs. The "slope" of the confining potential is herewith reduced. If we assume that a change in the depletion field ΔF_D will have approximately the same effect on E_{10} as a change of the induced field due to the back gate voltage ΔF_{BG}, then we can write that

$$\Delta E_{10}\approx\frac{\partial E_{10}}{\partial F_D}\Delta F_{BG}+\frac{\partial E_{10}}{\partial n}\Delta n\ , \tag{7}$$

and again with the values of Ref. 9 for E_{10} as a function of depletion field and carrier concentration, we obtain in this case the solid line of Fig. 7, in remarkably good agreement with the experimental data, when considering the approximations made for the electric fields.

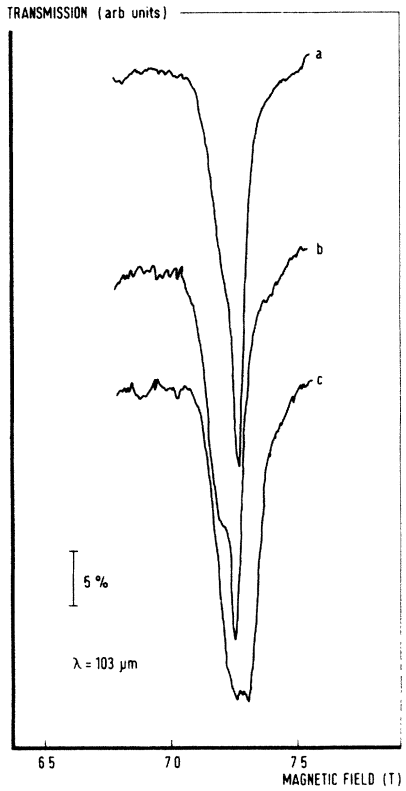

FIG. 8. Transmission at a laser wavelength $\lambda=103$ μm, showing the crossing of the $|0,2\rangle$ and $|1,0\rangle$ subband Landau levels, the "half-field" RSLC. The curves correspond to different values of the back gate voltage: (a) $V_g=-50$ V; (b) $V_g=0$ V; (c) $V_g=25$ V.

B. Laser measurements

The splitting of the CR observed in Fig. 1, can be qualitatively understood on the basis of Fig. 3, where we have shown the energy-level structure calculated for a small tilt angle θ. Near the anti-level-crossing, the eigenstates are linear combinations of the pure subband-Landau states [Eq. (2)] and the energy will deviate somewhat from the unperturbed value. Due to the mixing of the pure states, transitions will now be possible for incident FIR radiation of energy E_{10} at magnetic fields below and above the crossing, as long as the hybridized states have not been shifted by the coupling over much more than the level width. At fields too close to the crossing field, the shifts are larger and transitions will no longer be possible; at fields too far away, the mixing is negligible and transitions will no longer be possible because of the $\Delta N=1$ selection rule. And therefore, as curve b in Fig. 1, two absorption maxima can be found. A more quantitative explanation will be given in the next section.

An anti-level-crossing of the subband-Landau-levels has also been observed at 7.2 T, the "half-field," as shown in Fig. 8. At this magnetic field the filling factor for our samples with electron density cm^{-2} of typically 2×10^{11} is 1.5, so one expects a transition from the $|0,1\rangle$ state to a mixture of the $|0,2\rangle$ and $|1,0\rangle$ states. Therefore, the transition energy has only half the magnitude of the transition at full field, i.e., 12 meV. The splitting is considerably smaller for a comparable tilt angle. For example the

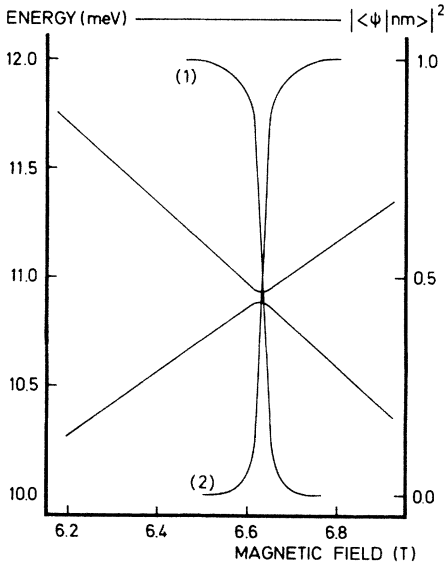

FIG. 9. The transition energy relative to the energy of the second Landau level of the lowest subband, calculated for a triangular well potential for $\theta=10°$, left-hand scale. Projections $|\langle\psi|n,m\rangle|^2$ of the eigenstates on the pure subband-Landau-level states $|n,N\rangle$, right-hand scale: (1), $|\langle\psi_2|0,2\rangle|^2$ and (2), $|\langle\psi_2|1,0\rangle|^2$. Within the resolution of this graph $|\langle\psi_3|1,0\rangle|^2=|\langle\psi_2|0,2\rangle|^2$ and $|\langle\psi_3|0,2\rangle|^2=|\langle\psi_2|1,0\rangle|^2$.

splitting ΔB of Fig. 1 at 14 T is 0.24 T, while the splitting of Fig. 8 at half-field, $\Delta B_{1/2}$, is 0.047 T. Calculations based on our triangular potential-well model also produce a much smaller splitting at the "half-field" crossing. Figure 9 illustrates the anti-level-crossing at the "half-field" where one considers the subband-Landau-level transitions from the $|0,1\rangle$ state to the hybridized $|0,2\rangle$ and $|1,0\rangle$ states. Note that unlike the case of Fig. 3, the transitions take place between levels with different Landau-level index; in Fig. 9 therefore $E_{10}-\hbar\omega_c$ is plotted, instead of a horizontal line E_{10} as in Fig. 3. The relative weakness of the coupling is due to the fact that the overlap of the wave functions belonging to the zeroth Landau level of the first excited subband $|1,0\rangle$ and to the second Landau level of the lowest subband $|0,2\rangle$ is smaller than the overlap of $|1,0\rangle$ with $|0,1\rangle$.

V. LINE BROADENING AND TRANSITION PROBABILITY

For a more quantitative analysis of the splitting of Fig. 1 we have calculated the transition probability using the wave functions ψ_i; for these calculations assumptions had to be made concerning the shape and broadening of the Landau levels near the anti-level-crossing.

The transition probability from the ground state to the mixed state at an energy E_f is calculated using Fermi's golden rule, where the electron-photon interaction is approximated by the electric dipole (ED) Hamiltonian:

$$P(\hbar\omega,B)=\frac{2\pi}{\hbar}\sum_f |\langle\psi_f|H_{\rm ED}|0,0\rangle|^2\delta(E_f-E_0-\hbar\omega)$$

$$=\frac{2\pi}{\hbar}\sum_f\sum_{n,N}|\langle\psi_f|n,N\rangle\langle n,N|H_{\rm ED}|0,0\rangle|^2$$

$$\times\delta(E_f-E_0-\hbar\omega)\ . \tag{8}$$

When the incident radiation is parallel to the magnetic field and only the most dominant projections are retained, i.e., those on $|0,1\rangle$ and $|1,0\rangle$, one finds from Eq. (8)

$$P(\hbar\omega,B)=\frac{2\pi E^2e^2}{\hbar}\sum_{f=1}^{2}|\sqrt{2}l_\perp\cos\theta\langle\psi_f|0,1\rangle+z_{10}\sin\theta\langle\psi_f|1,0\rangle|^2\delta(E_f-E_0-\hbar\omega)\ . \tag{9}$$

In order to be able to calculate the absorption line shape, we have to assign to each of the eigenfunctions ψ_i a line shape $F_i(\hbar\omega)$ with a width δ_i and to integrate Eq. (9) over the energy $\hbar\omega$.

A homogeneously broadened Lorentzian line shape gives very good agreement of the calculated absorption with the measured CR far away from the anti-level-crossing, with typical widths of 75 μeV. But with the assumption of such a Lorentzian broadening one still fails to reproduce the occurrence of two resonances at different values of the applied magnetic field as in Fig. 1. And indeed, one cannot expect that the line shape will remain Lorentzian near the anti-level-crossing because of the following arguments: Consider the perturbation expansion of the coupling due to H'; the first-order perturbation from the $\theta=0$ unperturbed energy will shift the energy of a broadened level without affecting its line shape. The second-order perturbation term, however, will cause a level repulsion which is biggest for energy levels that are closest together; consequently, for two sets of levels that would be broadened initially with a Lorentzian line shape, the difference in strength of the repulsion in the tails closest together and in the tails farther apart will cause the line shape near the anti-level-crossing to become asymmetric, in such a way that for ψ_1 the high-energy tail is steepened and for ψ_2 the low-energy tail. In order to be able to handle this analytically, we have assumed that the tails have a Gaussian shape. Figure 10 shows a typical example of the calculated absorption at an incident FIR energy equal to E_{10}, for different tilt angles. The calculated angle dependence is stronger than experimentally observed. But our calculations clearly show that when the broadening of the levels is taken into account the splitting observed in Fig. 1 can be accounted for.

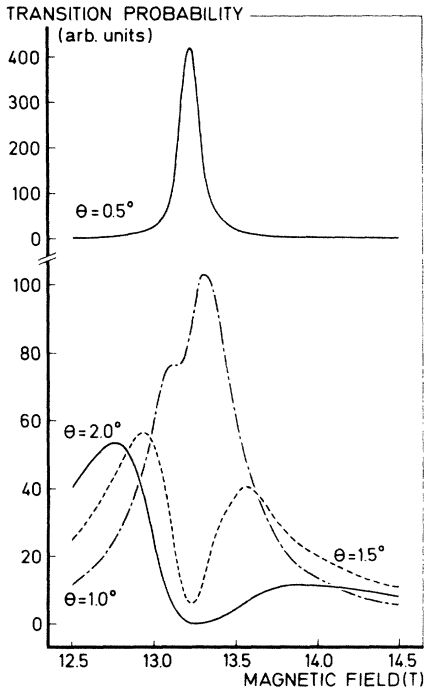

FIG. 10. Transition probability as a function of magnetic field calculated for $\hbar\omega=E_{10}=21.85$ meV and for various values of the tilt angle θ.

VI. SUMMARY AND CONCLUSIONS

We have observed splitting of the CR in a 2D EG due to resonant coupling of the $|0,1\rangle$ and $|1,0\rangle$, and of the

$|0,2\rangle$ and $|1,0\rangle$ subband Landau levels. This effect is observed in CR for fixed strength of the applied magnetic field and also for fixed energy of the incident radiation.

RSLC enables one to determine the subband transition energy E_{10} and to study its variation with the electric field at the interface. We have demonstrated how this variation depends on the manner by which the carrier density is changed: With increasing electron density due to a back gate voltage the subband transition energy E_{10} is lowered, while it will be raised by an increase in density due to photoexcitation of charge carriers.

We have shown that the coupling strength depends on the extension of the subband wave functions through the matrix elements z_{nm} and so gives valuable information on the shape of the interface potential.

We also showed that the resonances observed at fixed energy of incident radiation can be modeled with the wave functions calculated here using a Gaussian broadening of the Landau levels.

In conclusion, RSLC is a very sensitive method to test interface potential calculations, it allows the direct determination of the subband energy structure, and the coupling strength gives information on the spatial extension of the subband wave functions.

ACKNOWLEDGMENTS

Part of this work was supported by the Stichting voor Fundamenteel Onderzoek der Materie (FOM) with the financial support from the Nederlandse Organisatie voor Zuiver Wetenschappelijk Onderzoek (ZWO).

*Also at Hochfeld Magnetlabor, Max-Planck-Institut für Festkörperforschung, Boîte Postale No. 166X, F-38042 Grenoble Cédex, France.

†Present address: Max-Planck-Institut für Festköperforschung, D-7000 Stuttgart 80, Federal Republic of Germany.

[1]T. Ando, A. B. Fowler, and F. Stern, Rev. Mod. Phys. **54**, 437 (1982), and references therein.

[2]P. Kneschaurek, A. Kamgar, and J. F. Koch, Phys. Rev. B **14**, 1610 (1976), and references therein.

[3]B. D. McCombe, R. T. Holm, and D. E. Schafer, Solid State Commun. **32**, 603 (1979).

[4]W. Beinvogl and J. F. Koch, Phys. Rev. Lett. **40**, 1736 (1978).

[5]Z. Schlesinger, J. C. M. Hwang, and S. J. Allen, Phys. Rev. Lett. **50**, 2098 (1983).

[6]G. L. J. A. Rikken, H. W. Myron, C. J. G. M. Langerak, and H. Sigg, Surf. Sci. **170**, 160 (1986).

[7]G. Weimann and W. Schlapp, Appl. Phys. Lett. **46**, 411 (1985).

[8]G. L. J. A. Rikken, H. W. Myron, P. Wyder, G. Weimann, W. Schlapp, R. E. Horstman, and J. Wolter, J. Phys. C **18**, L175 (1985).

[9]F. Stern and S. Das Sarma, Phys. Rev. B **30**, 840 (1984).

[10]T. Ando, Phys. Rev. B **19**, 2106 (1979).

[11]It can be readily shown that any potential $V(z)$ with a simple power law λz^i (where i is an arbitrary number) will lead to matrix elements z_{nm} which do not depend on λ but only on i.

[12]M. Zaluzny, Solid State Commun. **55**, 747 (1985), **56**, 235 (1985).

[13]A. Kastalsky and J. C. M. Hwang, Solid State Commun. **51**, 317 (1984).

[14]B. Vinter, Solid State Commun. **48**, 151 (1983).